Synthesis and characterization of activated carbon-supported magnetic nanocomposite (MNPs-OLAC) obtained from okra leaves as a nanocarrier for targeted delivery of morin hydrate

Cem Öziç [1], Erdal Ertaş [2], Mehmet Fırat Baran [2], Ayşe Baran [3]*, Elham Ahmadian[4], Aziz Eftekhari [5,6]*, Rovshan Khalilov[7], Elvin Aliyev[8] and Mahmut Yıldıztekin [9]*

[1]Department of Basic Medical Sciences, Department of Medical Biology, Kafkas University, Faculty of Medicine, Kars, Türkiye, [2]Department of Food Technology, Vocational School of Technical Sciences, Batman University, Batman, Türkiye, [3]Department of Biology, Graduate Education Institute, Mardin Artuklu University, Mardin, Türkiye, [4]Kidney Research Center, Tabriz University of Medical Sciences, Tabriz, Iran, [5]Department of Biochemistry, Faculty of Science, Ege University, Izmir, Türkiye, [6]Department of Life Sciences, Western Caspian University, Baku, Azerbaijan, [7]Department of Biophysics and Biochemistry, Baku State University, Baku, Azerbaijan, [8]Department of Biology and Ecology, Lankaran State University, Lankaran, Azerbaijan, [9]Department of Herbal and Animal Production, Koycegiz Vocational School, Mugla Sıtkı Kocman University, Mugla, Türkiye

Introduction: The method of encapsulating the drug molecule in a carrier, such as a magnetic nanoparticle, is a promising development that has the potential to deliver the medicine to the site where it is intended to be administered. Morin is a pentahydroxyflavone obtained from the leaves, stems, and fruits of various plantsmainly from the Moraceae family exhibiting diverse pharmacological activities such as anti-inflammatory, anti-oxidant, and free radical scavenging and helps treat diseases such as diabetes, myocardial infarction and cancer.

Methods: In this study, we conducted the synthesis of a nanocomposite with magnetic properties by coating biocompatible activated carbon obtained from okra plant leaves with magnetic nanoparticles.

Results: Characterization of the synthesized activated carbon-coated magnetic nanocomposite was confirmed by Fourier transform infrared, scanning electron microscopy, dynamic light scattering, and zeta potential. The cytotoxic effects of the drug-loaded magnetic nanocomposite were examined in HT-29 (Colorectal), MCF-7 (breast), U373 (brain), T98-G (Glioblastoma) cancer cell lines, and human umbilical vein endothelial cells healthy cell line.

Discussion: We studied the loading and release behavior of morin hydrate in the activated carbon-coated magnetic nanocomposite. Activated carbon-coated magnetic nanocomposite carriers can show promising results for the delivery of Morin hydrate drugs to the targeted site.

KEYWORDS

morin hydrate, MCF-7, anticancer activity, magnetic nanocomposite, drug delivery

1 Introduction

Nano-sized materials exhibit a size distribution in the range of 1–100 nm and have a significant surface area, making them highly suitable for biological applications (Adepu and Ramakrishna, 2021; Talha et al., 2022; Mekuye and Abera, 2023). Magnetic nanoparticles (MNPs) have the potential to be used in biomedical settings for purposes like cancer cell imaging, controlled drug release, and hyperthermia treatment. The reason for this is that they have unique physical properties and their ability to interact biologically at the cellular level (Ali et al., 2021; Nasibova et al., 2023). MNPs have several advantageous properties, including their magnetic susceptibility, biocompatibility, stability, and the capacity to be prepared using multiple processes. Moreover, MNPs may be easily manipulated by an external magnetic field, enabling precise control over the release of cancer drugs in a specific location and at a desired rate. Thus, the difficulties encountered in traditional diagnosis and treatment can be overcome (Kush et al., 2021).

Morin hydrate (3,5,7,2′,4′-pentahydroxyflavone) is a yellowish bioflavonoid with versatile biological and pharmacological potential obtained from various plants, especially from the fruits, stems, and leaves of plants belonging to the Moraceae family (Mottaghi and Abbaszadeh, 2021). Many *in vivo* and *in vitro* experiments have reported that morin hydrate (MH) has significant healing potential with a wide range of pharmacological properties including anti-inflammatory, anti-oxidant, free radical scavenger in various diseases such as life-threatening cancer, cardiovascular anomalies, acute lung and liver injury, neuroinflammatory disorders, kidney complications, diabetes, gastritis, through its bioactivity mechanisms (Karamchedu et al., 2020; Balaga et al., 2023).

In this study, activated carbon-coated magnetic nanocomposite (MNPs@OLAC) was synthesized according to the co-precipitation method of interaction of activated carbon (AC) obtained from okra leaves (OL) with magnetic nanoparticles and loaded with MH. MNPs@OLAC magnetic nanocomposite was characterized by Fourier transform infrared spectroscopy (FTIR), scanning electron microscopy (SEM), dynamic light scattering (DLS), and zeta potential techniques. MH release from MNPs@OLAC magnetic nanocomposites under *in vitro* conditions was investigated and analyzed at different pH values and times. Finally, the effects of MH-loaded MNPs@OLAC magnetic nanocomposites on cell viability on the cytotoxicity of HT-29 (Colorectal), MCF-7 (breast), U373 (brain), T98-G (Glioblastoma) cancer cell lines and Human Umbilical Vein Endothelial Cells (HUVEC) healthy cell line were evaluated.

2 Materials and methods

2.1 Chemicals and reagents

Materials ferric chloride hexahydrate (≥99% purity), ferrous sulfate heptahydrate (≥99% purity), hydrochloric acid (37%, ACS reagent), sodium hydroxide (≥97.0%, pellets), ammonium hydroxide (≥28% purity), Morin hydrate (≥100% purity), methanol (≥99.8%, ACS reagent), dimethyl sulfoxide (DMSO) (≥99.9%, ACS reagent), ethanol (96%, ACS reagent)and zinc chloride (≥98% purity) were purchased from Sigma-Aldrich. All

other chemicals used were of analytical grade. Double-distilled water was used for synthesis, solution preparation, and other purposes throughout the experiment.

2.2 Characterization

2.2.1 Instruments

The synthesized MNPs@OLAC and MNPs@OLAC-MH were characterized to determine their structural characteristics and morphology using the following methods:

Scanning Electron Microscopy (SEM); Conducted using a QUANTA 400F instrument to examine the surface morphology of MNPs@OLAC and MNPs@OLAC-MH.

Zeta Potential: The stability of nanoparticles in solution was measured using a Zetasizer Nano ZS from Malvern Instruments Ltd. at 25°C.

Laser Particle Sizer; Particle agglomerate size distributions were evaluated using a Mastersizer 2000 Particle Size Analyzer from Malvern Instruments.

Fourier Transform Infrared Spectrophotometry (FT-IR); Functional groups present in MNPs@OLAC and MNPs@OLAC-MH were analyzed using a Perkin Agilent Cary 630 FTIR spectrometer.

UV-Visible Spectrophotometry: The UV–visible absorption spectrum was recorded using an Agilent Cary 60 Spectrophotometer.

Before taking measurements, the samples were obtained from the stock solution by diluting them with pure water as required.

2.3 Preparation of OLAC

The leaves of the okra plant were first washed with tap water several times and then washed and cleaned with deionized water 5 times to remove dust and contaminants adhering to the surface of the leaves. After the cleaning process, drying was done in the open air in a fume hood at room temperature, and the dried okra leaves were ground into a powder with the help of an IKA M20 Universal grinder and stored in a container to be used in OLAC production. 10 g of the powder sample obtained by grinding the leaves of the okra plant after drying were weighed, taken into a 500 mL erlenmayer, then, a solution of zinc chloride with a concentration of 1 M (for activation of activated carbon) was added and mixed in a shaking water bath at 80°C for 1 hour (Veerakumar et al., 2016). The precipitate of the mixture, which was brought to room temperature and cooled, was placed in a glass crystallization container to be homogeneous and dried in an oven at 100°C for 24 h. Afterward, the dried mixture was placed in porcelain crucibles and subjected to carbonization in the muffle furnace set at 600°C. The OLAC obtained after the carbonization process was cooled in a desiccator at 25°C. Washing was carried out several times with 0.1 N HCl to remove unreacted zinc, chlorine, and other ions on the surface of OLAC. After washing with HCl, the product was washed with deionized water (until the acidity was removed and the pH value became neutral) and left to dry in an oven at 70°C for 24 h (Farma et al., 2023; Komal et al., 2024).

2.4 Preparation of MNPs@OLAC nanocomposite

As reported in the literature, with some modifications, the surface of MNPs was synthesized by coating them with AC obtained from the okra plant (Inbaraj et al., 2021). 3.0 g of iron (III) chloride hexahydrate was dissolved in 50 mL of deionized water in an argon gas atmosphere. In the next step, 2.1 g of iron (II) sulfate heptahydrate was added to the solution containing Fe^{3+} ions and the temperature of the mixture was slowly increased to 90 °C in the presence of argon gas. After 30 min, 10 mL of 26% ammonium hydroxide solution was added to the mixture, and a black solution was formed. This resulting solution continued to be mixed in the magnetic stirrer for another 30 min under the same conditions. Then, 500 mg of OLAC solution dissolved in 100 mL of water was added to the mixture. After the addition of the solution containing OLAC, the product in the magnetic stirrer was mixed for 60 min and the resulting MNPs@OLAC nanocomposite was allowed to cool at room temperature, and the MNPs@OLAC nanocomposite was separated from the solution medium using a magnet. The MNPs@OLAC nanocomposite was washed several times with deionized water and dried in a lyophilizer. After the drying process, the MNPs@OLAC nanocomposite was stored in a colored container to be used in experimental studies.

2.5 Investigation of the loading and release conditions of morin hydrate

For the purpose of to loading MH into the MNPs@OLAC magnetic nanocomposite, 10 mL of a 100 µg/mL MH solution dissolved in methanol was added to 50 mg of the nanocomposite. The mixture was then stirred in a water bath at room temperature for 24 hoursThen, the particles were isolated from the solution using an external magnet based on their magnetic properties, and the MH concentration in the solution was measured at a wavelength of 385 nm using UV-Vis spectrophotometry. To calculate drug loading, it was obtained by subtracting the MH concentration in the supernatant from the initial MH concentration using Equation 1. Subsequently, magnetic nanoparticles which contained the medication were isolated by the application of a magnetic field and thereafter underwent a drying procedure.

Drug loading efficiency (%) =

$$\frac{\text{Total amount of drug} - \text{Free drug in the supernatant}}{\text{Total amount of drug}} \times 100$$

(1)

For the purpose of the MH release investigation, 10 mg of dry drug-loaded nanoparticles were analyzed in 5 mL of PBS with a pH of 5.4 and 7.4 at a temperature of 37 °C while being stirred for durations of 1, 3, 6, 12, 18, 24, 36, 48, 60, and 72 h. UV-Vis spectrophotometry was performed at a wavelength of 385 nm to determine the amount of medication that was released after the set incubation periods had passed During the course of the drug release tests, measurements were carried out in accordance with Equation 2.

$$\text{Drug release (\%)} = \frac{\text{Released drug}}{\text{Total drug}} \times 100$$

(2)

2.6 Cell viability test studies

An examination of the viability of the cells was conducted out at the Cell Culture Laboratory of the Dicle University Faculty of Veterinary Medicine Laboratory. The healthy cell line (HUVEC) and the cancer cell lines (MCF-7, U373, T98-G, and HT-29) were obtained from the "American Type Culture Collection" (ATCC).

In accordance with the findings of Baran, the chosen cell lines were grown in a cell culture medium contained within a T75 flask and then incubated at 37 °C in an atmosphere containing 5% carbon dioxide (Baran, 2023). After the cells had attained a confluency level of 80%–90%, they were removed from the flasks and the hemocytometric method was used to determine the total number of cells. To carry out two separate time applications, 24 and 48 h, the cells whose numbers were calculated were injected onto 96-well plates in sizes of 10×10^5 in three replicates, with 90 µL of media in each well. Additionally, the cells were inoculated into microplates in triplicate for MNPs@OLAC-MH in pH 7.4 and MNPs@OLAC-MH in pH 5.4 with the intention of doing two separate time applications. The cells were waited for 24 h to adhere to the microplate bottom. The next day, MNPs@OLAC-MH at pH 7.4 and MNPs@OLAC-MH at pH 5.4 were applied to the seeded plates at various concentrations (1, 50, 100, and 200 µg/mL). Liquid with pH 7.4 for MNPs@OLAC-MH and pH 5.4 for MNPs@OLAC-MH was applied to the cells in the control group.

MTT test was conducted at 24 and 48 h following the application, to assess alterations in cell viability. Each well-containing cells in the microplate was supplemented with 10 µL of the prepared MTT solution (5 mg/mL) and then incubated for 3 h at 37 °C in a humid atmosphere with 5% CO_2. Following a 3-h duration, the medium was removed and 100 µL of DMSO were added to each well. After a 20-min incubation period on the shaker, the optical density (OD) values of the wells were measured using UV/Vis Spectrophotometry (Schneider et al., 2021; Montazersaheb et al., 2024).

The average absorbance values obtained by reading the control wells were accepted as 100% live cell values. The absorbance values obtained from the MNPs@OLAC-MH in pH 7.4 and MNPs@OLAC-MH in pH 5.4 applied wells were accepted as % viability by proportioning them to the control absorbance value. MTT trials were repeated three times on different days.

2.7 Statistical analysis

The data collected from the study were analyzed using the IBM SPSS 21.0 software package. The statistical significance level was deemed acceptable at a p-value of less than 0.05. Data were compared between groups using unpaired t-tests and among multiple groups by one-way ANOVA, followed by Tukey's $post$ hoc tests. $P < 0.05$ was considered statistically significant.

3 Results and discussion

3.1 FT-IR analysis of MNPs@OLAC and MNPs@OLAC-MH nanocomposites

Figure 1 shows the characterization results of MNPs@OLAC and MNPs@OLAC-MH nanocomposites by FTIR spectroscopy.
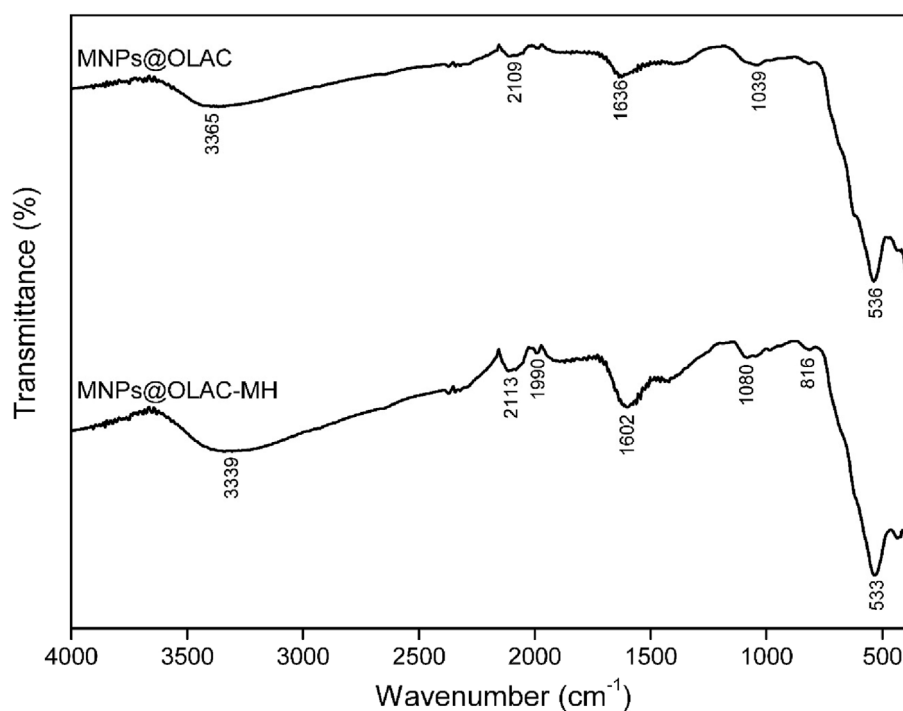
FIGURE 1
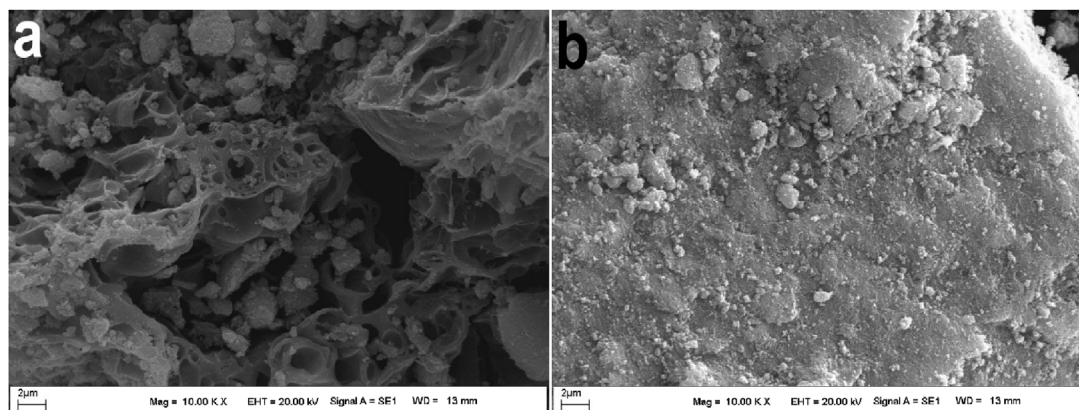FT-IR spectrometers MNPs@OLAC and MNPs@OLAC@MH.

FIGURE 2
SEM images of **(A)** MNPs@OLAC; **(B)** MNPs@OLAC-MH.

The FT-IR spectrum of MNPs@OLAC nanocomposite at 3365 cm^{-1} is attributed to the stretching and vibration of the–OH (alcoholic and phenolic) group (Ma et al., 2022). When the spectra of MNPs@OLAC and MNPs@OLAC-MH are examined, the peak at 2109 cm^{-1} corresponds to the C≡C stretching of alkynes (Emenike et al., 2023), when the spectrum of MNPs@OLAC and MNPs@OLAC-MH nanocomposites at 2113 cm^{-1} is examined, the measured peak is attributed to the presence of C-H and alkyne groups (Xavier, 2021; Mazumdar et al., 2015; Ferreira et al., 2017) and the peaks observed at 1990–1994 cm^{-1} indicate stretching vibration of C=C bonds (in alkynes) (Al and Kabakcı, 2024). The peaks seen at 1602 and 1636 cm^{-1} (C=O group) correspond to the presence of hydroxyl and carboxylic acid groups (Ezeonuegbu et al., 2021). In addition, for MNPs@OLAC and MNPs@OLAC@MH nanocomposites, the absorption of the peaks at 1039 and 1080 cm^{-1} indicates the presence of C-O and C-N groups (He et al., 2022; Sun et al., 2020). When the spectra of MNPs@OLAC and MNPs@OLAC@MH are examined in Figure 2, the peak seen at 533 and 536 cm^{-1} indicates the presence of Fe-O bond (Tural et al., 2024).
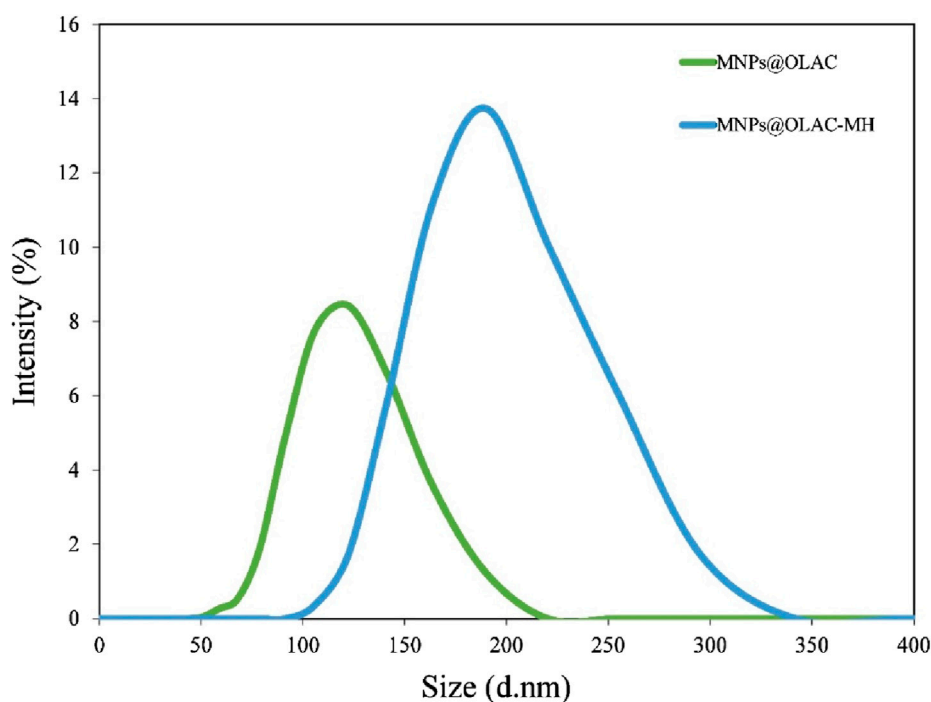
FIGURE 3
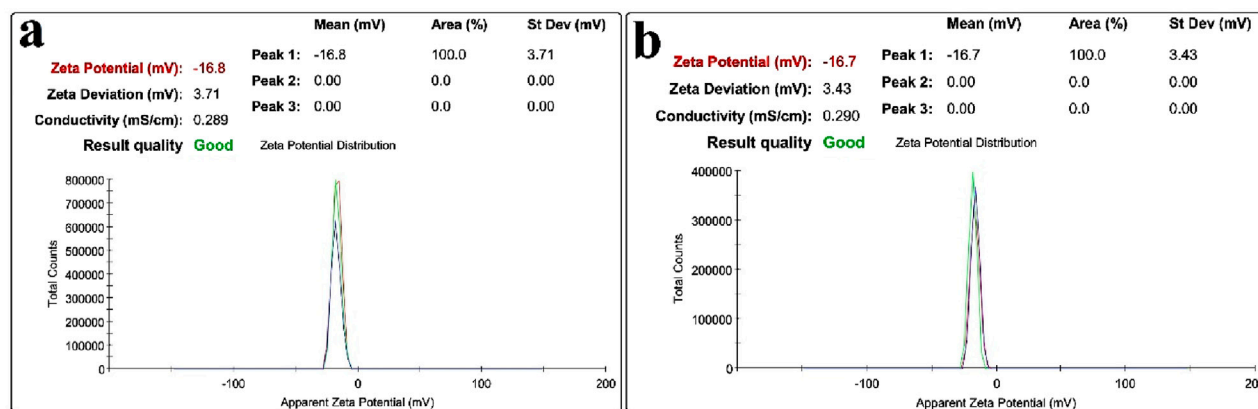Hydrodynamic diameters of MNPs@OLAC and MNPs@OLAC-MH determined by DLS.

FIGURE 4
Zeta potential for **(A)** MNPs@OLAC **(B)** MNPs@OLAC-MH.

3.2 SEM analysis of MNPs@OLAC and MNPs@OLAC-MH nanocomposites

The surface images of MNPs@OLAC and MNPs@OLAC-MH nanocomposites were analyzed using SEM. SEM images of MNPs@OLAC and MNPs@OLAC-MH nanocomposites are shown in Figures 2A, B. The MNPs@OLAC nanocomposite has different pore diameters and a granular surface. The reason for the smoothness on the surface of the MNPs@OLAC nanocomposite after the MNPs@OLAC-MH nanocomposite obtained after the MH drug was bound to the surface of the MNPs@OLAC nanocomposite

is due to the irregular distribution of the drug in the surface morphology and pore structures of the nanocomposite (Baig et al., 2022).

3.3 DLS analysis of MNPs@OLAC and MNPs@OLAC-MH

The DLS analysis results of MNPs@OLAC and MNPs@OLAC-MH nanocomposites are shown in Figure 3. Analyses were performed with the solution obtained by weighing 1 mg of the
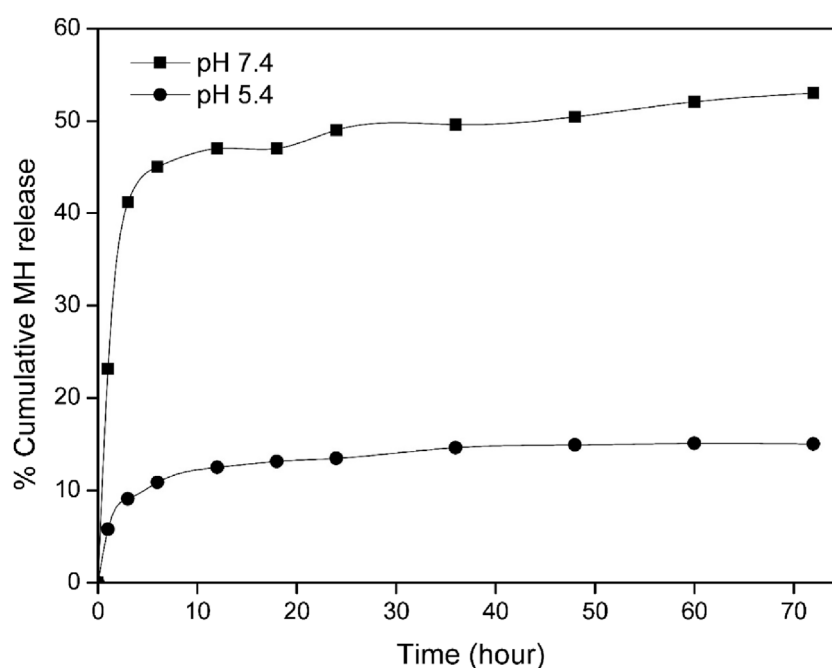
FIGURE 5
Comparative release profile of MH in MNPs@OLAC conjugated MH.

nanocomposite material and sonicating it in 10 mL of deionized water. When the results of the DLS analysis are examined, it is seen that MNPs@OLAC and MNPs@OLAC-MH nanocomposites have an average size distribution of 122 and 190 nm, respectively (Kovrigina et al., 2022).

3.4 The zeta-potential measurements of MNPs@OLAC and MNPs@OLAC-MH nanocomposites

The zeta potential analysis results of MNPs@OLAC and MNPs@OLAC-MH nanocomposites are shown in Figure 4. As a result of zeta potential measurement, information about the electric charge on the surface of any material is obtained. To prevent agglomeration of MNPs@OLAC and MNPs@OLAC-MH nanocomposites and to ensure stability between nanocomposites, it is desired to obtain either high positive or negative zeta potential values. The potential values of MNPs@OLAC and MNPs@OLAC-MH nanocomposites under the determined optimum conditions were measured as −16.8 and −16.7 mV, respectively. When the results are examined, it is seen that MNPs@OLAC and MNPs@OLAC-MH nanocomposites show low agglomeration due to their negatively charged value, and therefore the prepared suspensions maintain their stability for a long time (Attia et al., 2022).
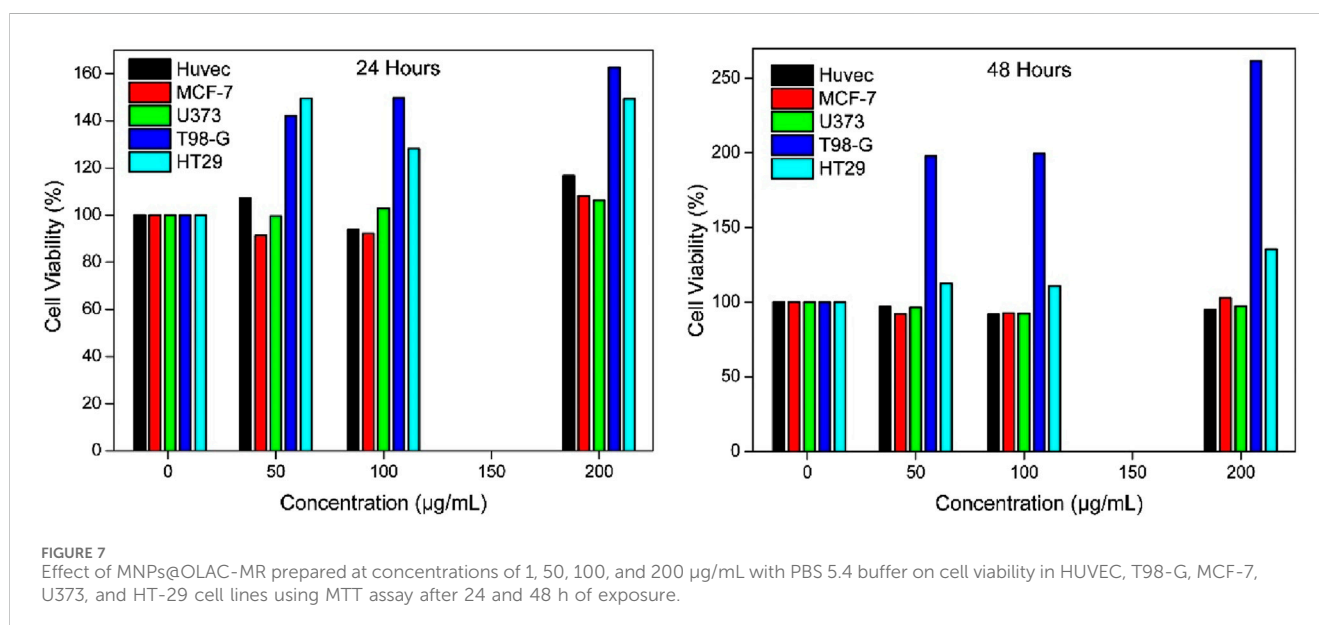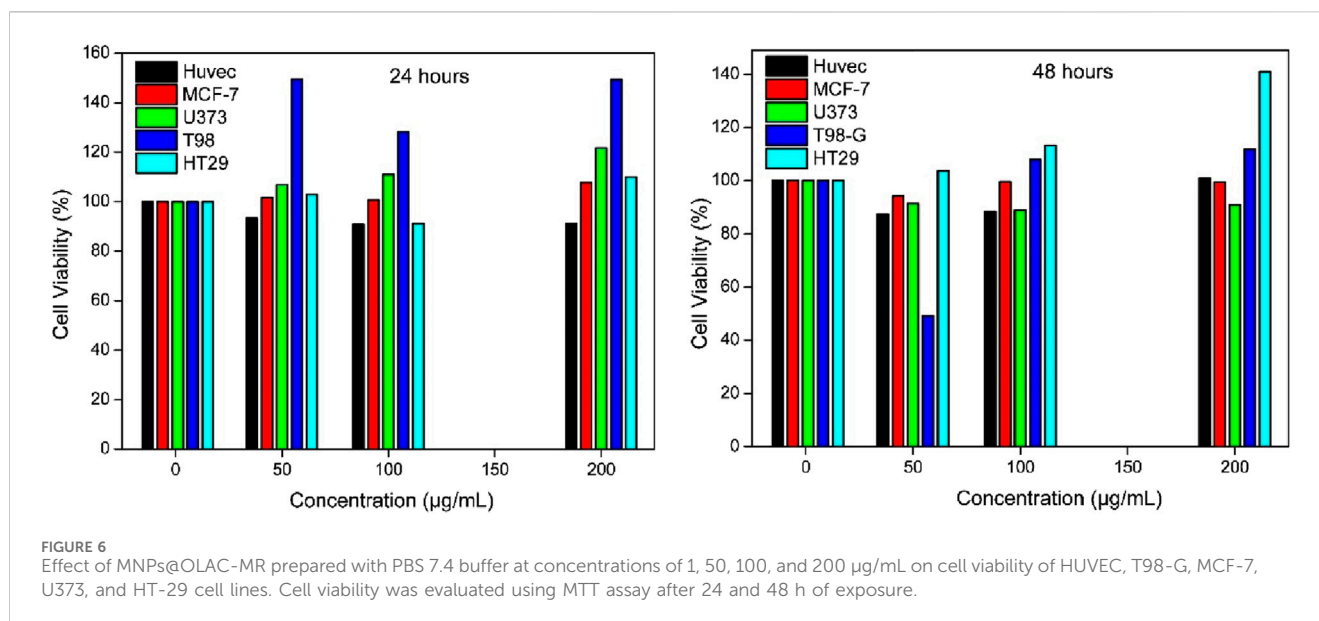
3.5 The behavior of pH-Dependent release

At a temperature of 37°C, Figure 5 illustrates the cumulative release of MH in MNPs@OLAC at pH 7.4 (the physiological pH)

and pH 5.4 (the acidic environment in tumor tissues). MH was found to be released more under physiological settings, and the release of MH changed determined by the pH value that was evaluated. This phenomenon was discovered when different pH values for MH release were investigated (Cunha et al., 2023). To perform the release studies, 10 mL solutions of 96 μg/mL MH loaded into MNPs@OLAC at different pH values and concentrations were used. The ratio of MR mass to the volume of the release medium was found to be 9.6 μg/mL. After 24 h, the release from bulk MH decreased from 48.98% at pH 7.4%–13.47% at pH 5.4. At pH 5.4, in the release of loaded MH in MNPs@OLAC, the release was 10.86% after 6 h, 12.48% after 12 h, 14.89% after 48 h, and 15.02% after 72 h (Kulkarni and Belgamwar, 2019; Jangid et al., 2020). At pH 7.4, in the release of loaded MH in MNPs@OLAC, the release was 45.04% after 6 h, 47.00% after 12 h, 50.44% after 48 h, and 53.01% after 72 h.

MCF-7 breast cancer model (Fuster et al., 2021), U373, HT-29 colon model (Singh et al., 2022), glioblastoma model (Jiang et al., 2024) and T98-G glioblastoma model (Long et al., 2022) cell lines have been widely used as in various studies. Furthermore, HUVEC was utilized as a healthy cell line throughout the course of this research. The MTT assay was utilized in order to examine the cytotoxic effects of MH loaded in MNPs@OLAC nanocomposites against the cell lines HT-29, MCF-7, U373, T98-G, and HUVEC.

Through the process of reduction, a tetrazolium compound (MTT) is transformed into formazan in the MTT test, which is a colorimetric assay that is extensively used (Lovato et al., 2024). For the purpose of determining cellular metabolic activity, which serves as an indicator of toxicity, colorimetric tests are utilized extensively (Abd AL-Hadi et al., 2024). The effect of MH release in pH 7.4 and 5.4 solutions of MNPs@OLAC-MH prepared in phosphate buffer on

FIGURE 6
Effect of MNPs@OLAC-MR prepared with PBS 7.4 buffer at concentrations of 1, 50, 100, and 200 μg/mL on cell viability of HUVEC, T98-G, MCF-7, U373, and HT-29 cell lines. Cell viability was evaluated using MTT assay after 24 and 48 h of exposure.

FIGURE 7
Effect of MNPs@OLAC-MR prepared at concentrations of 1, 50, 100, and 200 μg/mL with PBS 5.4 buffer on cell viability in HUVEC, T98-G, MCF-7, U373, and HT-29 cell lines using MTT assay after 24 and 48 h of exposure.

cell viability of HT-29, MCF-7, U373, T98-G, and HUVEC cell lines was evaluated after 24 and 48 h. Interaction with MH-loaded MNPs@OLAC nanocomposites at pH 7.4 for 24 h (Figure 6) did not cause significant differences in the viability of tested HT-29, MCF-7, U373, and T98-G cells and was significantly above the concentration ranges of tested MNPs@OLAC-MH for 24 h. However, as seen in Figure 6, after 48 h of interaction, 50 ug/mL concentration and T98-G showed an effect on cell viability.

Effect of MNPs@OLAC-MR (1–200 μg/mL prepared with PBS 7.4 buffer) on cell viability of HUVEC cell line, T98-G cell line, MCF-7 cell line, U373 cell line, and HT-29 cell line. Cell viability was assessed using MTT assay after 24 and 48 h of exposure.

When exposed to MH-loaded MNPs@OLAC nanocomposites at pH 5.4 for 24 and 48 h, the viability of the evaluated HT-29,

MCF-7, U373, and T98-G cells did not show any significant alterations (Figure 7). The concentration ranges of MNPs@OLAC-MH at 24 and 48 h were notably greater than the concentration ranges determined for the tested MNPs@OLAC-MH.

4 Conclusion

In this study, we synthesized MNPs@OLAC magnetic nanocomposites that will serve as the transporter of MH, an anticancer drug. MNPs@OLAC nanocomposite was characterized by techniques FTIR, SEM, DLS, and Zeta potential. Morin hydrate was successfully loaded into MNPs@OLAC magnetic nanocomposites using 24 24-h incubation technique. When both

pH 5.4 and pH 7.4 were compared, the increase in MH release at pH 7.4 was better for the release studies due to the encapsulation efficiency of MH, possibly due to the effect of increasing both the solubility and dissolution rate of the MH drug due to its transformation into a different form after loading into MNPs@ OLAC magnetic nanocomposites. This suggests that MH-loaded MNPs@OLAC magnetic nanocomposites may be a promising nano delivery system to treat HT-29, MCF-7, U373, and T98-G. MNPs@ OLAC-MH showed cytotoxic effects on cell viability in T98-G and U373 glioblastoma cell lines, MCF-7 lung cell lines, and HT-29 colon cell lines, both in concentration and time-dependent manner. In particular, T98-G cell lines showed more sensitivity in cell viability compared to U373, MCF-7, and HT-29 cells.

Data availability statement

The original contributions presented in the study are included in the article/supplementary material, further inquiries can be directed to the corresponding author.

Author contributions

CÖ: Writing–original draft, Visualization, Methodology, Investigation, Formal Analysis, Conceptualization. EE: Writing–original draft, Visualization, Methodology, Formal Analysis, Conceptualization. MB: Writing–original draft, Validation, Resources, Methodology, Investigation, Formal Analysis, Data curation, Conceptualization. AB: Writing–original draft, Resources, Project administration, Methodology, Conceptualization. EA: Writing–review and editing, Supervision, Resources, Project administration, Conceptualization. AE: Writing–review and editing, Supervision, Resources, Project administration, Conceptualization. RK: Writing–review and editing, Visualization, Validation, Supervision, Investigation. EA: Writing–review and editing, Visualization, Validation, Software, Methodology. MY: Writing–original draft, Writing–review and editing, Methodology, Data curation, Formal analysis, Project administration, Resources, Visualization.

Conflict of interest

The authors declare that the research was conducted in the absence of any commercial or financial relationships that could be construed as a potential conflict of interest.

Publisher's note

All claims expressed in this article are solely those of the authors and do not necessarily represent those of their affiliated organizations, or those of the publisher, the editors and the reviewers. Any product that may be evaluated in this article, or claim that may be made by its manufacturer, is not guaranteed or endorsed by the publisher.

References

Abd AL-Hadi, M. M., Ali, A. J., Marweh, A. K., Mohsen, R. J., and Bsio, H. S. (2024). Immune responses of mammals to foreign nanomaterials, oxidative stress and inflammation assays, toxicity of nanomaterials to living cells, and nanomedicine applications. *J. Curr. Med. Res. Opin.* 7 (06), 2716–2733. doi:10.52845/CMRO/2024/7-6-11

Adepu, S., and Ramakrishna, S. (2021). Controlled drug delivery systems: current status and future directions. *Molecules* 26 (19), 5905. doi:10.3390/molecules26195905

Al, K., and Kabakcı, S. B. (2024). Oxygen-rich precursors via glycerol organosolv treatment: preparation of activated carbon from hazelnut shell and its structural components for possible use in electrodes for supercapacitors. *Int. J. Thermofluids* 21, 100588. doi:10.1016/j.ijft.2024

Ali, A., Shah, T., Ullah, R., Zhou, P., Guo, M., Ovais, M., et al. (2021). Review on recent progress in magnetic nanoparticles: synthesis, characterization, and diverse applications. *Front. Chem.* 9, 629054. doi:10.3389/fchem.2021.629054

Attia, M., Glickman, R. D., Romero, G., Chen, B., Brenner, A. J., and Ye, J. Y. (2022). Optimized metal-organic-framework based magnetic nanocomposites for efficient drug delivery and controlled release. *J. Drug Deliv. Sci. Technol.* 76, 103770. doi:10.1016/j.jddst.2022.103770

Baig, M. M. F. A., Fatima, A., Gao, X., Farid, A., Khan, M. A., Zia, A. W., et al. (2022). Disrupting biofilm and eradicating bacteria by Ag-Fe3O4@MoS2 MNPs nanocomposite carrying enzyme and antibiotics. *J. Control Release* 352, 98–120. doi:10.1016/j.jconrel.2022.10.009

Balaga, V. K. R., Pradhan, A., Thapa, R., Patel, N., Mishra, R., and Singla, N. (2023). Morin: a comprehensive review on its versatile biological activity and associated therapeutic potential in treating cancers. *Pharmacol. Res. - Mod. Chin. Med.* 7, 100264. doi:10.1016/j.prmcm.2023.100264

Baran, A. (2023). Inhibitory effects of gold nanoparticles biosynthesized by redox reaction using *Rheum ribes* lam. fruit peels on pathogen strains and cancer cells. *Part. Sci. Technol.* 41 (7), 978–989. doi:10.1080/02726351.2023.2164875

Cunha, C., Marinheiro, D., Ferreira, B. J., Oliveira, H., and Daniel-da-Silva, A. L. (2023). Morin hydrate encapsulation and release from mesoporous silica nanoparticles for melanoma therapy. *Molecules* 28 (12), 4776. doi:10.3390/molecules28124776

Emenike, E. C., Odimayomi, K. P., Iwuozor, K. O., Ndagi, M., and Adeniyi, A. G. (2023). Synthesis of activated carbon monolith from lignocellulosic material: evaluation of product quality. *MRS Adv.* 8 (15), 816–822. doi:10.1557/s43580-023-00584-4

Ezeonuegbu, B. A., Machido, D. A., Whong, C. M. Z., Japhet, W. S., Alexiou, A., Elazab, S. T., et al. (2021). Agricultural waste of sugarcane bagasse as efficient adsorbent for lead and nickel removal from untreated wastewater: biosorption, equilibrium isotherms, kinetics and desorption studies. *Biotechnol. Rep.* 30, e00614. doi:10.1016/j.btre.2021.e00614

Farma, R., Julita, R. I., Apriyani, I., Awitdrus, A., and Taer, E. (2023). ZnCl$_2$-assisted synthesis of coffee bean bagasse-based activated carbon as a stable material for high-performance supercapacitors. *Mater. Today Proc.* 87, 25–31. doi:10.1016/j.matpr.2023.01.370

Ferreira, F. V., Franceschi, W., Menezes, B. R. C., Brito, F. S., Lozano, K., Coutinho, A. R., et al. (2017). Dodecylamine functionalization of carbon nanotubes to improve dispersion, thermal and mechanical properties of polyethylene based nanocomposites. *Appl. Surf. Sci.* 410, 267–277. doi:10.1016/j.apsusc.2017.03.098

Fuster, M. G., Carissimi, G., Montalbán, M. G., and Víllora, G. (2021). Antitumor activity of rosmarinic acid-loaded silk fibroin nanoparticles on HeLa and MCF-7 cells. *Polym* 13 (18), 3169. doi:10.3390/polym13183169

He, L., Shi, Y., Chen, Y., Shen, S., Xue, J., Ma, Y., et al. (2022). Iron-manganese oxide loaded sludge biochar as a novel periodate activator for thiacloprid efficient degradation over a wide pH range. *Sep. Purif. Technol.* 288, 120703. doi:10.1016/j.seppur.2022.120703

Inbaraj, B. S., Sridhar, K., and Chen, B. H. (2021). Removal of polycyclic aromatic hydrocarbons from water by magnetic activated carbon nanocomposite from green tea waste. *J. Hazard. Mater.* 415, 125701. doi:10.1016/j.jhazmat.2021.125701

Jangid, A. K., Agraval, H., Gupta, N., Jain, P., Yadav, U. C., Pooja, D., et al. (2020). Amorphous nano morin outperforms native molecule in anticancer activity and oral bioavailability. *Drug Dev. Ind. Pharm.* 46 (7), 1123–1132. doi:10.1080/03639045.2020.1776318

Jiang, M. Q., Yu, S. P., Estaba, T., Choi, E., Berglund, K., Gu, X., et al. (2024). Reprogramming glioblastoma cells into non-cancerous neuronal cells as a novel anti-cancer strategy. *Cells* 13 (11), 897. doi:10.3390/cells13110897

Karamchedu, S., Tunki, L., Kulhari, H., and Pooja, D. (2020). Morin hydrate loaded solid lipid nanoparticles: characterization, stability, anticancer activity, and bioavailability. *Chem. Phys. Lipids* 233, 104988. doi:10.1016/j.chemphyslip.2020.104988

Komal, Singh, R., Parale, V. G., Kumar, Y., Mishra, K., and Shukla, V. K. (2024). Studies on the $ZnCl_2$ activated carbons derived from Sabal palmetto and Pterospermum acerifolium leaves for EDLC application. *Biomass Convers. biorefin.* 14 (9), 9995–10009. doi:10.1007/s13399-022-03088-7

Kovrigina, E., Chubarov, A., and Dmitrienko, E. (2022). High drug capacity doxorubicin-loaded iron oxide nanocomposites for cancer therapy. *Magnetochemistry* 8 (5), 54. doi:10.3390/magnetochemistry8050054

Kulkarni, A. D., and Belgamwar, V. S. (2019). Influence of novel carrier Soluplus® on aqueous stability, oral bioavailability, and anticancer activity of Morin hydrate. *Dry. Technol.* 37 (9), 1143–1161. doi:10.1080/07373937.2018.1488261

Kush, P., Kumar, P., Singh, R., and Kaushik, A. (2021). Aspects of high-performance and bio-acceptable magnetic nanoparticles for biomedical application. *Asian J. Pharm. Sci.* 16 (6), 704–737. doi:10.1016/j.ajps.2021.05.005

Long, C., Yuan, L., Wei, W., and Li, J. (2022). Overcoming chemoresistance in glioblastoma by fluvastatin via prenylation-dependent inhibition of Ras signaling. *Hum. Exp. Toxicol.* 41, 09603271221125934. doi:10.1177/09603271221125934

Lovato, M. J., De Lama-Odría, M. D. C., Puiggalí, J., del Valle, L. J., and Franco, L. (2024). A color indicator based on 3-(4, 5-Dimethylthiazol-2-yl)-2, 5-diphenyltetrazolium bromide (MTT) and a biodegradable poly (ester amide) for detecting bacterial contamination. *Int. J. Mol. Sci.* 25 (12), 6671. doi:10.3390/ijms25126671

Ma, Y., Zhao, H., Ma, Q., Cheng, D., Zhang, Y., Wang, W., et al. (2022). Development of chitosan/potato peel polyphenols nanoparticles driven extended-release antioxidant films based on potato starch. *Food packag. Shelf Life* 31, 100793. doi:10.1016/j.fpsl.2021.100793

Mazumdar, P., Rattan, S., and Mukherjee, M. (2015). Polymer nanocomposites using click chemistry: novel materials for hydrogen peroxide vapor sensors. *RSC Adv.* 5 (85), 69573–69582. doi:10.1039/C5RA10952C

Mekuye, B., and Abera, B. (2023). Nanomaterials: an overview of synthesis, classification, characterization, and applications. *Nano Sel.* 4 (8), 486–501. doi:10.1002/nano.202300038

Montazersaheb, S., Eftekhari, A., Shafaroodi, A., Tavakoli, S., Jafari, S., Baran, A., et al. (2024). Green-synthesized silver nanoparticles from peel extract of pumpkin as a potent radiosensitizer against triple-negative breast cancer (TNBC). *Cancer nano.* 15, 47. doi:10.1186/s12645-024-00285-z

Mottaghi, S., and Abbaszadeh, H. (2021). The anticarcinogenic and anticancer effects of the dietary flavonoid, morin: current status, challenges, and future perspectives. *Phytother. Res.* 35 (12), 6843–6861. doi:10.1002/ptr.7270

Nasibova, A., Khalilov, R., Bayramov, M., Mustafayev, I., Eftekhari, A., Abbasov, M., et al. (2023). Electron paramagnetic resonance studies of irradiated grape snails (helix pomatia) and investigation of biophysical parameters. *Molecules* 28 (4), 1872.

Schneider, M. G. M., Favatela, M. F., Medina, G. A. M., van Raap, M. B. F., and Lassalle, V. L. (2021). Multitherapy magnetic theranostic: synthesis, characterization and *in vitro* evaluation of their performance. *Colloids Surf. B Biointerfaces.* 198, 111460. doi:10.1016/j.colsurfb.2020.111460

Singh, P., Waghambare, P., Khan, T. A., and Omri, A. (2022). Colorectal cancer management: strategies in drug delivery. *Expert Opin. Drug Deliv.* 19 (6), 653–670. doi:10.1080/17425247.2022.2084531

Sun, D., Li, P., Li, X., and Wang, X. (2020). Protein-resistant surface based on zwitterion-functionalized nanoparticles for marine antifouling applications. *New J. Chem.* 44 (5), 2059–2069. doi:10.1039/C9NJ04266K

Talha, M., Islam, N. U., Zahoor, M., Sadiq, A., Nawaz, A., Khan, F. A., et al. (2022). Biological evaluation, phytochemical screening, and fabrication of Indigofera linifolia leaves extract-loaded nanoparticles. *Molecules* 27, 4707.

Tural, B., Ertaş, E., Enez, B., and Tural, S. (2024). Removal lead (II) and toluidine blue from wastewater with new magnetic Bacillus niacini nano-biosorbent: lead and toluidine blue removal by magnetic Bacillus niacini nano-biosorbent. *Int. J. Environ. Sci. Technol.* 21 (11), 7431–7444. doi:10.1007/s13762-024-05515-w

Veerakumar, P., Panneer Muthuselvam, I., Hung, C. T., Lin, K. C., Chou, F. C., and Liu, S. B. (2016). Biomass-derived activated carbon supported Fe_3O_4 nanoparticles as recyclable catalysts for reduction of nitroarenes. *ACS Sustain. Chem. and Eng.* 4 (12), 6772–6782. doi:10.1021/acssuschemeng.6b01727

Xavier, J. R. (2021). Corrosion protection performance and interfacial interactions of polythiophene/silanes/MnO_2 nanocomposite coatings on magnesium alloy in marine environment. *Int. J. Polym. Anal. Charact.* 26 (4), 309–329. doi:10.1080/1023666X.2021.1887627